Tuning between the metallic antiferromagnetic and ferromagnetic phases of $La_{1-x}Sr_xMnO_3$ near $x=0.5$ by digital synthesis

Tiffany S. Santos,[1] Steven J. May,[2] J. L. Robertson,[3] and Anand Bhattacharya[1,2]
[1]*Center for Nanoscale Materials, Argonne National Laboratory, Argonne, Illinois 60439, USA*
[2]*Materials Science Division, Argonne National Laboratory, Argonne, Illinois 60439, USA*
[3]*Spallation Neutron Source, Oak Ridge National Laboratory, Oak Ridge, Tennessee 37831, USA*
(Received 4 March 2009; published 8 October 2009)

We investigated cation-ordered $La_{1-x}Sr_xMnO_3$ about the half-doping level $x\sim0.5$ in superlattices of alternating, single-unit-cell layers of $LaMnO_3$ and $SrMnO_3$. The effect of La/Sr cation order was addressed by comparing the structural, magnetic and transport properties of these superlattices with random-alloy films of equivalent composition. The samples were synthesized by ozone-assisted molecular-beam epitaxy onto $SrTiO_3$ substrates. The superlattices could be tuned between ferromagnetic and antiferromagnetic metallic states by inserting extra single-unit-cell layers of $LaMnO_3$ and $SrMnO_3$, respectively. For $x<0.5$, a ferromagnetic, metallic phase was observed. For $x=0.50$ and 0.55, *A*-type antiferromagnetic order was confirmed by neutron diffraction, with a Néel temperature of 300 K, significantly higher than bulk values. The enhanced Néel temperature was attributed to lattice strain rather than cation order.

DOI: 10.1103/PhysRevB.80.155114 PACS number(s): 75.70.Cn, 75.47.Lx, 61.05.fj, 73.21.Cd

I. INTRODUCTION

The interplay between charge, spin, orbital, and lattice degrees of freedom in the perovskite manganites gives rise to a wide spectrum of electronic and magnetic behavior. The coupled interactions between these degrees of freedom became of great importance because of their role in the colossal magnetoresistance (CMR) phenomenon—the insulator-metal transition accompanying the paramagnetic to ferromagnetic phase transition and a "colossal" response to external magnetic field, in several mixed-valence manganites.[1] Disorder of the cations on the *A* sites affects the temperature at which this phase transition occurs. The transition temperature not only varies with the dopant concentration and mean *A*-site cation radius, but decreases linearly with the variance of the cation size.[2,3] Furthermore, studies of bulk single crystals of $Ln_{0.5}Ba_{0.5}MnO_3$ (Ln=rare earths) found that cation ordering on the *A*-site gives rise to electronic and magnetic phases that are entirely absent in the disordered analogs.[4] In the case of $La_{0.5}Ba_{0.5}MnO_3$, *A*-site ordering was found to enhance the Curie temperature (T_C) from 270 K (*A*-site disordered) to 335 K.[5] Studies of ordered analogs in bulk crystals have been limited to compounds containing Ba (due to its large cation radius) and that too only near $x=0.5$. Using state-of-the-art techniques that enable atomic level precision in the synthesis of superlattices of complex oxides, it is possible to explore the effects of cation ordering for a broad range of compounds and compositions.

Our study concentrates on the $La_{1-x}Sr_xMnO_3$ (LSMO) system, which has a rich structural, electronic and magnetic phase diagram in bulk, crystalline form.[6] *A*-type antiferromagnetic (AF) and orbitally ordered, insulating $LaMnO_3$ (LMO) is on one end of the phase diagram, and *G*-type AF, insulating $SrMnO_3$ (SMO) is on the other. By varying the Sr doping (x), a wide range of properties, including ferromagnetic (*F*)-insulating, *F*-metallic, AF-metallic, and AF-insulating ground states, are displayed. Having a perovskite ABO_3 structure, crystals and thin films of LSMO typically have La and Sr atoms randomly distributed on the *A*-sites. In contrast to this disordered arrangement, in this study the La and Sr atoms are ordered along the growth direction in superlattices (SLs) of LMO and SMO. With the added influence of lattice strain due to epitaxial contraints to the $SrTiO_3$ substrate, the magnetic and transport properties can be tailored in LMO/SMO superlattices, in both the AF (Refs. 7 and 8) and *F* regime.[9–15] Our interest lies in the region near the $x=0.5$ doping level containing the *F*-AF phase transition, particularly the role of *A*-site disorder in nucleating the *F* or AF state. Our approach is to digitally combine undoped, unit-cell layers of SMO and LMO, in epitaxial SLs having an overall composition in the range of $0.44<x<0.55$.

Slightly Sr-rich LSMO ($0.5<x<0.6$) has an AF, metallic ground state. Homogeneous bulk single crystals in this composition range are challenging to synthesize due to nucleation of a hexagonal $SrMnO_3$ impurity phase.[16] Layer-by-layer growth of epitaxial SLs is a nonequilibrium synthesis technique that circumvents this complication. However, synthesizing this AF-metallic phase in thin-film form has also proven to be quite challenging, as it has a *F* metallic phase on one side and a strongly insulating phase on the other. Hence, attaining the correct doping level and oxygen content is crucial. Most previous attempts have produced samples with either appreciable magnetic moment, high resistivity or even insulating behavior,[10,15,17,18] and none have measured the AF structure.[19] Our digital synthesis method using ozone-assisted molecular-beam epitaxy (ozone MBE) enables us to achieve the AF-metallic state and to study the influence of La/Sr site order and lattice strain. The AF-metallic state is intriguing because antiferromagnets are usually insulating. Moreover, this one in particular has an *A*-type spin structure, characterized by *F* order of the Mn cations within the MnO_2 planes and AF order of adjacent MnO_2 planes. Within each plane, the spin-polarized charge carriers are delocalized via a double-exchange mechanism, while transport between planes is nominally forbidden. A material with such a spin structure in thin-film form may be incorporated into a spintronic device as a channel for spin transport.

 ©2009 The American Physical Society

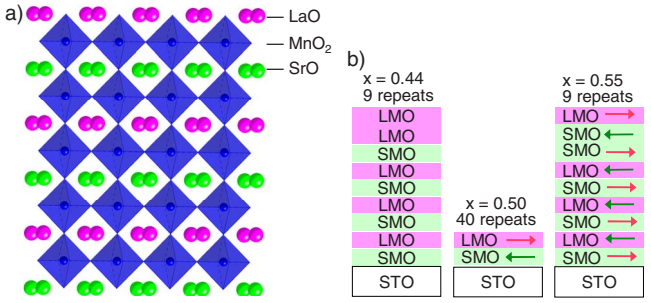

FIG. 1. (Color online) Schematic of a digital SL comprised of alternating, single-unit-cell layers of $LaMnO_3$ and $SrMnO_3$, maintaining an epitaxial, perovskite crystalline structure (a). The octahedrons represent the sixfold coordination of oxygen atoms around each centrally located Mn atom. Pink and green spheres represent the La and Sr atoms, respectively. (b) Layer stacking sequence of the SLs, showing a single supercell that is repeated the indicated number of times. The arrows denote the *A*-type AF spin structure.

II. EXPERIMENTAL

Using ozone MBE, we have taken an unique approach to fabricating LSMO compositions in the vicinity of $x=0.5$, in which La/Sr site disorder has been greatly reduced. For example, the $x=0.50$ composition was digitally synthesized by alternating the deposition of single-unit-cell layers of SMO and LMO (shown in Fig. 1), forming a SL with the structure $[SMO_1/LMO_1]_{40}$ in which the SMO_1/LMO_1 bilayers are repeated 40 times. To synthesize the $x=0.55$ composition, an extra SMO layer was inserted among the SMO_1/LMO_1 bilayers, forming a SL with the structure $[(SMO_1/LMO_1)_4SMO_1]_9$. Similarly, the $x=0.44$ composition has an extra LMO layer: $[(SMO_1/LMO_1)_4LMO_1]_9$. The films were prepared on insulating $SrTiO_3$ (STO) substrates, and the thickness was kept constant at 80 or 81 unit-cell layers ($\sim$30 nm) for all films in this study.

The structural, magnetic and transport properties of these films were compared with each other and fully epitaxial, random alloys of equivalent composition. The reflection high-energy electron-diffraction (RHEED) patterns of the sample surface were obtained *in situ* during film growth using an electron gun operated at 10 kV. The x-ray reflectivity spectra were measured using a 4-axis diffractometer ($\lambda=0.154\ 18$ nm) with a parallel-plate collimator, and the diffraction spectra were measured using a 4-bounce high-resolution monochromator ($\lambda=0.154\ 06$ nm). Magnetic moment (M) as a function of applied magnetic field (H) and temperature (T) was measured using a superconducting quantum interference device (SQUID) magnetometer. The neutron-diffraction measurements were carried out using the HB-1A triple-axis spectrophotometer at the High Flux Isotope Reactor at Oak Ridge National Laboratory.

A. Sample synthesis

The films were synthesized in a MBE chamber with a base pressure of $\sim 3\times 10^{-10}$ Torr. Pure, distilled ozone was used as the oxidizing agent to ensure a fully oxygenated film. A steady flow of ozone was delivered to the chamber from a water-cooled nozzle aimed at the substrate, maintaining the pressure at 2.0×10^{-6} Torr during source rate measurements and film growth. The ozone flux at the substrate was estimated to be between 3×10^{14} and 9×10^{14} $cm^{-2}\ s^{-1}$. La, Sr, and Mn (99.9% pure) were deposited from dual-filament Knudsen cells. All the Knudsen cells are differentially pumped so that the heated source materials are exposed to a partial ozone pressure $\sim 2\times 10^{-7}$ Torr when ozone is delivered to the growth chamber. Prior to film growth, the deposition rate of each source material was measured in ozone over the course of three hours using a quartz-crystal thickness monitor (QCM). Then the substrate was heated to the growth temperature of 690 °C, as determined by a pyrometer with emissivity correction. The shutters of the source materials were opened to deposit a single-unit-cell layer (typically 25–40 s), with a brief anneal (30 s) between each unit-cell layer. LMO (SMO) was deposited by coevaporation of La and Mn (Sr and Mn). The random-alloy films where deposited by coevaporation of La, Sr, and Mn. The shutter time for each material was determined by the rate measurements, and the shutters were automated with an open/close time <0.1 s. When deposition was complete, the sample was cooled to room temperature in ozone. The deposition rates of the source materials were measured again post-growth, with drift of the rates typically $<\pm 1\%$ per hour. Taking the drift into account, the La, Sr and Mn content of the films match the nominal composition to within ± 1 atomic percent.

Though we do not have a direct measure of oxygen content, we presume that our films are nearly stoichiometric for the following reason. Films with the doping level $x=0.50$ and 0.55 are very close to the F/AF phase boundary. Oxygen vacancies result in electron doping, which would cause the nominally AF composition to become ferromagnetic and have a higher magnetic moment. Our $x=0.50$ and 0.55 films show robust AF behavior (described in Sec. IV) with nearly zero moment, indicating that the films are not oxygen deficient.

Prior to film deposition, the STO (001) substrates were rinse in deionized water and then etched with a buffered hydroflouric acid (10 NH_4F:1 HF) for $\sim$20 s to prepare a TiO_2-terminated surface for epitaxial film growth.[20] For accurate measurement of the substrate temperature by pyrometry, 100 nm Pt was sputter deposited onto the back of the substrates. No adhesive was used to mount the substrate in the chamber.

B. Atomic flux calibration

A temperature-stabilized QCM was used to measure the deposition rate of each source material, with an error in the range of 0.5–0.8 % for La, Mn, and Sr. In order to calibrate the QCM rates, Rutherford backscattering spectroscopy (RBS) was used to determine the composition of $La_{1-x}Sr_xMnO_3$ films deposited on MgO substrates. RBS spectra were obtained using He^{++} particles with an incident energy of 2.3 MeV. The spectra were fit using SIMNRA software[21] to obtain the relative concentrations of La, Sr, and Mn within an error of 2% (upper bound, depending on total

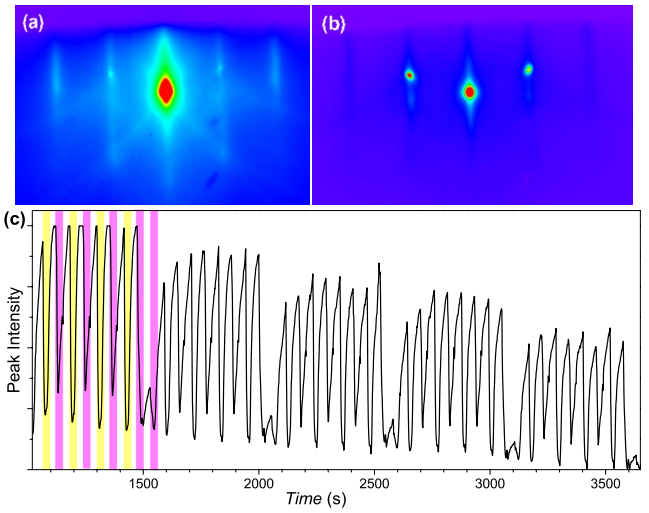

FIG. 2. (Color online) RHEED pattern of the STO substrate surface before film deposition (a) and of the $[(SMO_1/LMO_1)_4LMO_1]_9$ superlattice surface at the end of deposition (b), with the incident electron beam parallel to the [100] axis. Oscillations of the specular peak intensity (c) for the deposition of five supercells: pink and yellow regions mark the shutter-open times for LMO and SMO unit-cell layers, respectively, separated by 30 s anneal times.

number of counts). To obtain the absolute atomic fluxes, the thickness of a $LaMnO_3$ film on $SrTiO_3$ was determined using x-ray reflectivity to within 1% error. By combining these, a scaling constant was obtained for each element to convert the measured QCM rate to the atomic flux, which was then used to determine the shutter times for each source material prior to every film growth. The atomic flux at the substrate was between 1.5×10^{13} and 3.2×10^{13} cm^{-2} s^{-1}.

III. STRUCTURAL CHARACTERIZATION

As determined in the study of single-crystalline $La_{1-x}Sr_xMnO_3$ by Hemberger *et al.*,[6] the crystal structure at room temperature changes from rhombohedral at $x=0.5$ (with $a=0.546$ nm and $\alpha=60.16°$), to tetragonal at $x=0.55$ (with $a=0.544$ and $c=0.775$). At these compositions when lowering the temperature, the structure undergoes a transition to a monoclinic phase, accompanying a magnetic transition from a ferromagnetic metal at high temperature to an antiferromagnetic metal at low temperature. They found indications of a structurally mixed phase in the AF metal regime. The $x=0.44$ composition is expected to be a rhombohedral, ferromagnetic metal with $T_C=355$ K.[6,22] Because our LSMO films and SLs are grown epitaxially on STO substrates, they have a nominally tetragonal structure with $c/a<1$. Our detailed characterization of the film and surface structure by RHEED, x-ray reflectivity (XRR) and x-ray diffraction (XRD) is described in this section.

The structure of the surface layer of the film was monitored *in situ* during growth using RHEED. Figures 2(a) and 2(b) show the RHEED pattern collected with the incident electron beam parallel to the [100] axis, for both the STO substrate surface prior to film growth and the SMO/LMO

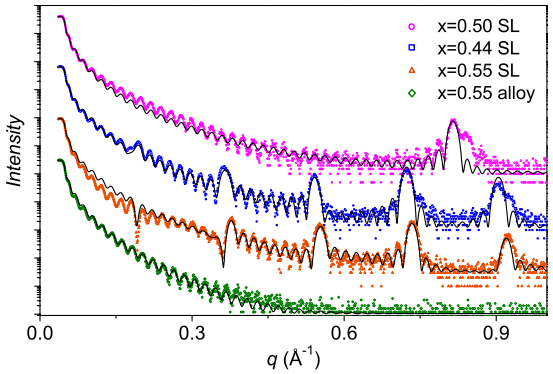

FIG. 3. (Color online) X-ray reflectivity of digitally synthesized SMO/LMO superlattices, with $x=0.50$ (alternating SMO and LMO layers), $x=0.55$ (inserting an additional SMO) and $x=0.44$ (inserting an additional LMO). The black lines for each spectrum are the fit calculated using Parratt's dynamical formalism. The spectra are offset for clarity.

film surface after growth was completed. The intense specular and first-order spots are indicative of a highly ordered, two-dimensional (2D) surface layer. Deep oscillations of the specular spot intensity during growth of the $x=0.44$ SL are shown in Fig. 2(c), over a time period of five supercells (repeated unit containing nine layers: $[SMO_1/LMO_1]_4LMO_1$), indicating layer-by-layer growth mode. The amplitude of the oscillations gradually decays, signifying a slight roughening of the film with increasing thickness. The roughness of the interfaces and surface is quantified in our XRR analysis.

Atomic layer control of our digital synthesis technique is demonstrated in our structural characterization by XRR, shown in Fig. 3 plotted versus momentum transfer $q(Å^{-1})$. A single Bragg peak in the XRR of the $x=0.50$ SL results from the different densities of SMO and LMO in the repeated SMO_1/LMO_1 bilayer, and is not present in the $x=0.44$ and 0.55 SLs. Rather, several other peaks appear due to the additional LMO or SMO layer and the resultant nine-layer supercell. Importantly, these strong SL peaks would not appear if there was intermixing at the interfaces on the order of a unit cell. The $x=0.55$ random alloy has a homogeneous density profile and thus has no SL peaks, as expected. Parratt's dynamical formalism[23] was used to fit these XRR spectra, with layer thickness, density and roughness as fit parameters. The following values were found for all SLs, over all the compositions in this study. All layer roughness of the SLs were <0.1 nm. The roughness of the top surface layer, to which the XRR is most sensitive, was <0.2 nm. The densities of the SMO and LMO layers in the SLs were between 5.5 and 5.7 g/cm^3 and between 6.5 and 6.7 g/cm^3, respectively. Thickness of the single-unit-cell layers were between 0.370 and 0.374 nm for SMO and between 0.395 and 0.397 nm for LMO, closely matching the out-of-plane lattice parameters for SMO and LMO found in a previous study.[7] The SMO and LMO are strained in the *a-b* plane to the STO substrate ($a_{STO}=0.3905$ nm), leading to tensile strain in the *a-b* plane for SMO and compressive strain for LMO.

From our XRD measurements, the (002) diffraction peaks of the SLs are shown in Fig. 4. The average *c*-axis parameter,

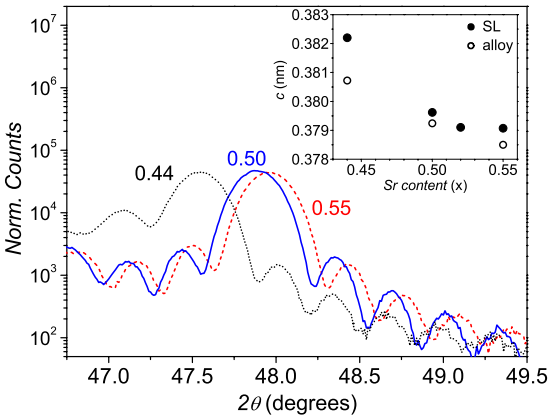

FIG. 4. (Color online) XRD (002) peaks of the SLs, showing a smaller, average c-axis parameter as the Sr content increases. The smaller peaks at higher and lower 2θ are thickness fringes. The inset shows the average c-axis as a function of Sr content, for both the SLs and alloys.

shown in the inset of Fig. 4 decreases with Sr content for both the SLs and random-alloy films. The dependence of c on Sr content is not linear, but decreases more abruptly between the $x=0.44$ and $x=0.5$ SLs, with smaller change for $x>0.5$. This may be correlated with $d_{x^2-y^2}$ orbital occupancy above $x=0.5$. A high degree of out-of-plane crystallinity was determined by the full width at half maximum (FWHM) of the rocking curve at the (002) peak position. The widths of the rocking curves (RCs) ranged from 0.045 to 0.065° for the SLs and from 0.037 to 0.042° for the random-alloy films. For reference, the RC widths of the STO substrates ranged from 0.022 to 0.033°. A ϕ-scan of the (101) peaks (not shown) verified the fourfold symmetry of the film matching that of the STO substrate, with the cube-on-cube, epitaxial relationship [100]film ∥ [100]STO and [001]film ∥ [001]STO.

Table I lists the results from the XRR and XRD analysis of the SLs. A small error in thickness, ranging from −0.5% to 1.5%, is shown when comparing the supercell thickness d found from XRR and c found from XRD. This error originates from the deviation of d/c from the nominal number of unit cells per supercell.

IV. MAGNETIC PROPERTIES

The magnetic behavior in the LSMO system results from a compromise between two coupling interactions among the $Mn^{3+/4+}$ ions—AF superexchange and F double exchange. The superexchange interaction of the localized t_{2g} electrons between neighboring Mn ions, mediated by the oxygen atoms, leads to AF coupling of the spins. The double-exchange interaction, mediated by the itinerant e_g electrons, leads to F coupling. The relative strength of these interactions is dependent on the lattice strain induced by the coherent epitaxy to the STO substrate.[19]

In our films, the a-b plane is under tensile strain, with $c/a<1$, and the films with higher Sr content have a smaller average c-axis parameter (see Fig. 4 inset). Such a distortion favors occupancy of the $d_{x^2-y^2}$ orbitals lying in the a-b plane. The carriers are delocalized within the MnO_2 sheets, thus minimizing energy.[16,24,25] At the same time, AF superexchange coupling of the t_{2g} electrons persists along the c axis and should be stronger for shorter distances between MnO_2 planes. The resulting behavior is the A-type AF ground state, in which the spins within the MnO_2 sheets are ferromagnetically aligned and adjacent sheets are antiferromagnetically aligned. On the La-rich side of the phase diagram ($x<0.5$), for which there is a larger c/a ratio, LSMO is in an orbitally disordered ($d_{3z^2-r^2}/d_{x^2-y^2}$ hybridized) state, allowing for double exchange in all three dimensions. The F-AF transition as the Sr content is varied from $x=0.44$ to $x=0.55$ is manifested in the magnetic characterization of our SLs and alloy films, as described in the following section.

A. Magnetization measurements

$M(T)$ of the SLs is shown in Fig. 5(a), along with comparisons of the SL and alloy for each composition [Figs. 5(b)–5(d)]. The $x=0.44$ films shows ferromagnetic behavior, as expected for La-rich LSMO, with $T_C=305$ K. The T_C is lower than that of bulk $La_{0.56}Sr_{0.44}MnO_3$ (355 K),[6,22] which is typical of ferromagnetic LSMO epitaxial films and attributed to lattice strain.[26] The saturation moment (M_S) of the alloy film and the SL is 2.2 μ_B and 1.7 μ_B per Mn ion, respectively, as found by $M(H)$ measurement (not shown). The lower M_S of the SL may result from a modulated magnetic profile,[17,27] having a higher moment in regions of the SL close to the double LMO layer and a lower moment in between the double LMO layers, or it could be due to a canted A-type AF order. The $M(T)$ measurement of the $x=0.50$ and 0.55 films show a highly reduced moment, consistent with AF order in these SLs, which is further addressed by our neutron-diffraction study.

TABLE I. XRD and XRR analysis of the SLs. t is the total film thickness determined by XRR; c is the average c-axis parameter measured by XRD; and d is the supercell thickness determined by XRR. The FWHM of the RC was measured at the (002) peak.

Sample	x	t (nm)	c (nm)	d (nm)	d/c	No. of u.c./supercell	% error	RC (deg)
0016	0.55	30.51	0.3791	3.46	9.13	9	1.44	0.047
0018	0.52	28.50	0.3791	7.15	18.9	19	−0.53	0.065
0020	0.50	31.11	0.3796	0.77	2.03	2	1.50	0.046
0030	0.44	30.92	0.3822	3.48	9.11	9	1.22	0.053

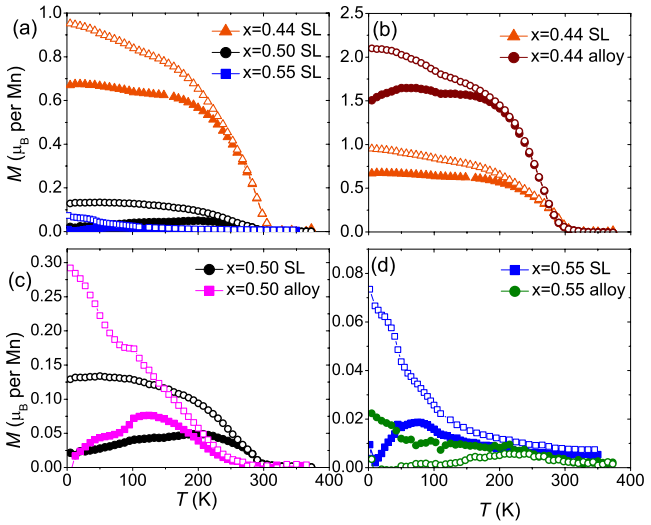

FIG. 5. (Color online) (a) $M(T)$ of the SLs, zero-field cooled (solid symbols) and cooled in 200 Oe field (open symbols). (b)–(d)$M(T)$ of the SLs compared with alloy films of equivalent composition. $M(T)$ was measured while increasing T in 200 Oe field.

B. Neutron diffraction

Neutron diffraction measurements were carried out on the SLs and alloys in order to determine the AF spin structure. The structurally forbidden $(0\ 0\ \frac{1}{2})$ Bragg peak emerged [shown in Figs. 6(a) and 6(c)] below the Néel temperature (T_N) for the $x=0.50$ and 0.55 SLs and alloys, corresponding to A-type AF order, which manifests itself as a doubling of

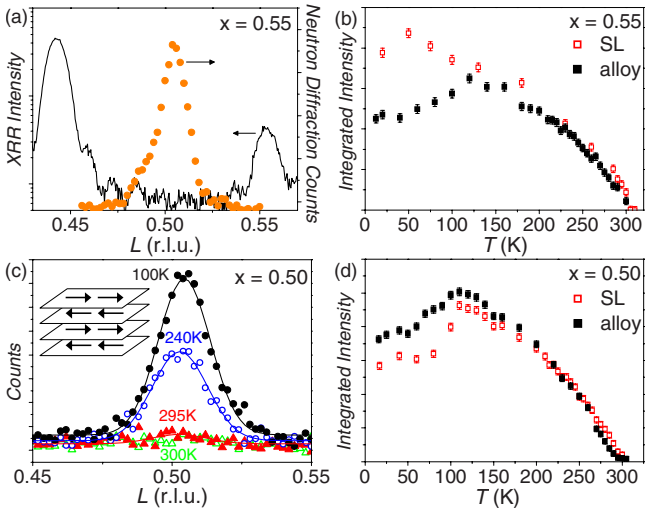

FIG. 6. (Color online) (a) The structurally forbidden $(0\ 0\ \frac{1}{2})$ neutron-diffraction peak (circles) of the $x=0.55$ SL, between structural, x-ray peaks (black line, from Fig. 3), confirming A-type AF order. (b) Temperature dependence of the $(0\ 0\ \frac{1}{2})$ peak intensity for the $x=0.55$ SL and random alloy, both revealing T_N significantly greater than that of bulk. (c) Neutron diffraction $(0\ 0\ \frac{1}{2})$ peak at the indicated temperatures for the $x=0.50$ SL. The inset is a schematic of the spin order on the MnO_2 planes that produces the $(0\ 0\ \frac{1}{2})$ peak. (d) Temperature dependence of the peak intensity for the $x=0.50$ SL and random alloy, both showing $T_N \sim 300$ K.

the unit cell along the c axis. Remarkably, the integrated intensity of a $(0\ 0\ L)$ scan through the $(0\ 0\ \frac{1}{2})$ peak as a function of T [shown in Figs. 6(b) and 6(d)] revealed a $T_N = 300$ K, which is a significant enhancement over the bulk alloy value of 220 K.[6,18,28] A magnetic coherence length equal to the film thickness was determined from the FWHM of the diffraction peaks for the SLs and alloy films, meaning that the alternating spin orientations on the MnO_2 planes persist through the entire film thickness. One would expect a nuclear peak for the $x=0.50$ SL at $L=0.5$ for $T>T_N$. However, its intensity is too weak to be observed.[29] The structural phase transition of the STO substrate[30] at 105 K, from cubic to tetragonal, causes the lower integrated peak intensity at low T observed for all of the films.

For bulk samples with $x=0.50$ and 0.55, the A-type AF phase transforms into a F phase at approximately 220 K, which then has a T_C of 330 and 280 K, respectively.[6,28] Our neutron-diffraction results, combined with the $M(T)$ measurements, indicate that the high-temperature F phase is absent in our films. The A-type AF phase remains stable all the way up to 300 K before long-range magnetic order is lost. Furthermore, since the SLs and alloy films show the same T_N, this suggests that strain, rather than cation order, causes stabilization of the AF phase and the observed enhancement of T_N over that of the bulk compound. This is in contrast to the result of May *et al.*,[8] who showed a T_N value of 320 K for a $x=2/3$ superlattice, approximately 70 K higher than that of the $x=2/3$ random-alloy film. In that study, the alloy film is strongly insulating, with a resistivity several orders of magnitude greater than the SL. In contrast, the films in the present study are nearly metallic, having much lower resistivity. Presumably, the small increase in resistivity due to A-site disorder near $x=0.5$ (see below) is not sufficient to weaken double-exchange F order in plane, so that there is nearly no observable change in T_N value with cation disorder.

Surprisingly, even though the $x=0.44$ SL displayed a relatively large magnetization with a $T_C=305$ K when measured in a SQUID magnetometer [see Fig. 5(b)], this SL also has a $(0\ 0\ \frac{1}{2})$ neutron-diffraction peak (not shown). The coexistence of a sizable magnetic moment and a $(0\ 0\ \frac{1}{2})$ AF peak can result from a canted spin structure. The results on the $x=0.44$ SL will be reported elsewhere.[31]

V. TRANSPORT PROPERTIES

The resistivity (ρ) of the films correlates with the magnetic properties. The ρ as a function of T and H, shown in Fig. 7, was measured using a 4-point probe technique with the magnetic field applied in the plane of the film. The SLs display a clear trend of increasing ρ with hole doping, from 0.07 mΩ-cm for the $x=0.44$ SL to 2 mΩ-cm for the $x=0.55$ SL at 5 K [Fig. 7(a)]. This is in agreement with the general trend for the LSMO system of transitioning from a metallic F state to an insulating AF state with increasing Sr content beyond $x=0.5$. In the AF state our SLs indeed show primarily metallic behavior, i.e., decreasing ρ with decreasing T, though $\rho(T)$ increases for $T<50$ K in some cases. The metallic behavior in the A-type AF state results from

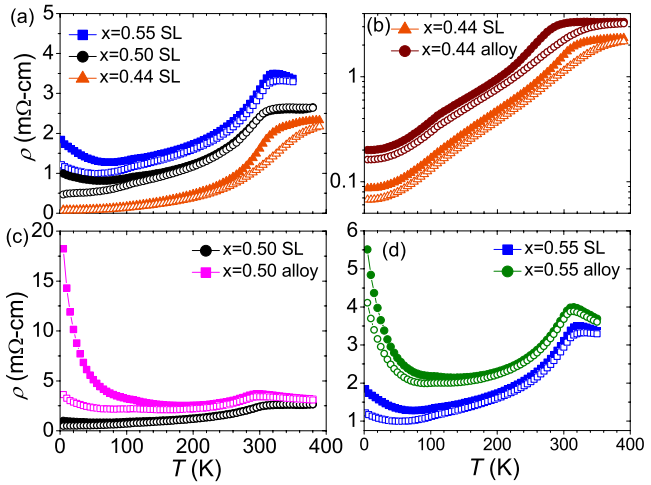

FIG. 7. (Color online) (a) $\rho(T)$ of the SLs, measured in zero magnetic field (solid symbols) and in 7 T field (open symbols). (b)–(d) $\rho(T)$ of the SLs compared with the alloy films of equivalent composition.

high conductivity of spin-polarized carriers via double-exchange hopping in the in-plane $d_{x^2-y^2}$ orbitals. Thus, the carriers are confined to the MnO_2 sheets.

The ρ decreases when a magnetic field is applied. This could be due to a reduction of in-plane spin scattering, if the AF domains align such that the AF spins are perpendicular to the applied field direction (i.e., spin flop). In addition, ρ can also be reduced by field-induced canting of the AF-coupled spins on adjacent planes, allowing electron hopping along the c axis.[32] Sizable magnetoresistance remaining at low T is characteristic of the AF metal films,[17,19] in contrast to the ferromagnetic $x=0.44$ films that show little MR at low T but CMR at higher T near T_C. We note that the upturn at low T is entirely eliminated for the $x=0.50$ SL with a 7 T magnetic field, and ρ decreases monotonically down to the lowest T measured.

As seen in Figs. 7(b)–7(d), all of the alloy films are higher in resistivity compared to the corresponding SL. The higher ρ values may simply be due to the lower mobility of the carriers in the alloy films, caused by the chemical disorder. As a result of the random distribution of La and Sr ions on the A sites of the alloy films, the conduction electrons (whether in the metallic F state or confined to the MnO_2 sheets as in the AF metal case) are subjected to a nonperiodic Coulomb potential, local lattice distortions and random variations in bond angles. Thus, the carriers in the alloy have a higher probability for scattering compared to those in the SLs.[4]

In addition to an overall higher ρ for the alloys in comparison to the SLs, the effect of disorder is also manifested in the increase in ρ at low T. Transport in the 2D $d_{x^2-y^2}$ bands is very sensitive to disorder, and the carriers become strongly localized at low T, resulting in a rise in ρ that is more pronounced for the random-alloy films with $x=0.50$ and 0.55 compositions, as compared to the SLs.

VI. CONCLUSIONS

Using ozone MBE, we have synthesized $LaMnO_3/SrMnO_3$ digital superlattices that span the F to AF phases of $La_{1-x}Sr_xMnO_3$ about $x=0.5$, while maintaining a high degree of cation order on the A-sites. The ferromagnetic samples at $x=0.44$ show evidence for coexistence of F and AF order, which may arise from canting of an A-type AF. For $x \geq 0.5$ A-type AF order in both the SLs and alloy films sets in with $T_N=300$ K, much higher than in bulk LSMO, and the F phase present above T_N in bulk LSMO is eliminated. Because the T_N value is the same for both ordered and disordered structures, the stabilization of the AF phase is attributed to lattice strain, rather than to cation order. We speculate that the enhanced T_N value results from compression of the c axis due to tensile strain in the a-b plane, which causes greater overlap of the t_{2g} orbitals, and consequently stronger superexchange along the c axis. The effect of La/Sr disorder is evident in the higher resistivity of the alloy films compared to the SLs, and carrier localization at low temperatures, but this does not influence the ordering temperatures.

In the A-type AF-metallic thin films, the $d_{x^2-y^2}$ orbital occupancy gives rise to in-plane spin-polarized transport that is isolated from adjacent planes of opposite spin polarity. These 2D bands could potentially provide separate channels for transport of spin-up and spin-down carriers. Furthermore, the lack of chemical disorder in the SLs reduces the probability for spin scattering and prevents an increase in resistivity at low temperature due to disorder-induced localization. These strained films have an enhanced T_N, extending this useful spin structure through a wider temperature range.

ACKNOWLEDGMENTS

Use of the Center for Nanoscale Materials was supported by the U.S. Department of Energy, Office of Science, Office of Basic Energy Sciences, under Contract No. DE-AC02-06CH11357. T.S. is supported by the CNM. S.M. and A.B. acknowledge the support of the Digital Synthesis FWP at MSD, Argonne. A portion of this research at Oak Ridge National Laboratory's High Flux Isotope Reactor was sponsored by the Scientific User Facilities Division, Office of Basic Energy Sciences, U.S. Department of Energy. We thank Jerel Zarestky for help with the measurements at HFIR and Suzanne te Velthuis for helpful discussions.

[1] A.-M. Haghiri-Gosnet and J.-P. Renard, J. Phys. D **36**, R127 (2003).

[2] L. M. Rodriguez-Martinez and J. P. Attfield, Phys. Rev. B **54**, R15622 (1996).

[3] L. M. Rodriguez-Martinez and J. P. Attfield, Phys. Rev. B **58**, 2426 (1998).

[4] D. Akahoshi, M. Uchida, Y. Tomioka, T. Arima, Y. Matsui, and Y. Tokura, Phys. Rev. Lett. **90**, 177203 (2003).

[5] F. Millange, V. Caignaert, B. Domengès, and B. Raveau, Chem. Mater. **10**, 1974 (1998).
[6] J. Hemberger, A. Krimmel, T. Kurz, H.-A. Krug von Nidda, V. Y. Ivanov, A. A. Mukhin, A. M. Balbashov, and A. Loidl, Phys. Rev. B **66**, 094410 (2002).
[7] A. Bhattacharya, X. Zhai, M. Warusawithana, J. N. Eckstein, and S. D. Bader, Appl. Phys. Lett. **90**, 222503 (2007).
[8] S. J. May, P. J. Ryan, J. L. Robertson, T. S. Santos, S. G. E. te Velthuis, J.-W. Kim, E. Karapetrov, J. N. Eckstein, S. D. Bader, and A. Bhattacharya (to be published).
[9] P. A. Salvador, A.-M. Haghiri-Gosnet, B. Mercey, M. Hervieu, and B. Raveau, Appl. Phys. Lett. **75**, 2638 (1999).
[10] T. Koida, M. Lippmaa, T. Fukumura, K. Itaka, Y. Matsumoto, M. Kawasaki, and H. Koinuma, Phys. Rev. B **66**, 144418 (2002).
[11] H. Yamada, M. Kawasaki, T. Lottermoser, T. Arima, and Y. Tokura, Appl. Phys. Lett. **89**, 052506 (2006).
[12] S. J. May, A. B. Shah, S. G. E. te Velthuis, M. R. Fitzsimmons, J. M. Zuo, X. Zhai, J. N. Eckstein, S. D. Bader, and A. Bhattacharya, Phys. Rev. B **77**, 174409 (2008).
[13] A. Bhattacharya, S. J. May, S. G. E. te Velthuis, M. Warusawithana, X. Zhai, B. Jiang, J.-M. Zuo, M. R. Fitzsimmons, S. D. Bader, and J. N. Eckstein, Phys. Rev. Lett. **100**, 257203 (2008).
[14] C. Adamo, P. S. X. Ke, A. Soukiassian, M. Warusawithana, L. Maritato, and D. G. Schlom, Appl. Phys. Lett. **92**, 112508 (2008).
[15] H. Nakao, J. Nishimura, Y. Murakami, A. Ohtomo, T. Fukumura, M. Kawasaki, T. Koida, Y. Wakabayashi, and H. Sawa, J. Phys. Soc. Jpn. **78**, 024602 (2009).
[16] T. Akimoto, Y. Maruyama, Y. Moritomo, A. Nakamura, K. Hirota, K. Ohoyama, and M. Ohashi, Phys. Rev. B **57**, R5594 (1998).
[17] M. Izumi, T. Manako, Y. Konishi, M. Kawasaki, and Y. Tokura, Phys. Rev. B **61**, 12187 (2000).
[18] P. K. Muduli, S. K. Bose, and R. C. Budhani, J. Phys.: Condens. Matter **19**, 226204 (2007).
[19] Y. Konishi, Z. Fang, M. Izumi, T. Manako, M. Kasai, H. Kuwahara, M. Kawasaki, K. Terakura, and Y. Tokura, J. Phys. Soc. Jpn. **68**, 3790 (1999).
[20] G. Koster, B. L. Kropman, G. J. H. M. Rijnders, D. H. A. Blank, and H. Rogalla, Appl. Phys. Lett. **73**, 2920 (1998).
[21] M. Mayer, *SIMNRA User's Guide 6.04* (Max-Planck-Institut für Plasmapysik, Germany, 2008).
[22] Y. Moritomo, T. Akimoto, A. Nakamura, K. Ohoyama, and M. Ohashi, Phys. Rev. B **58**, 5544 (1998).
[23] L. G. Parratt, Phys. Rev. **95**, 359 (1954).
[24] H. Kawano, R. Kajimoto, H. Yoshizawa, Y. Tomioka, H. Kuwahara, and Y. Tokura, Phys. Rev. Lett. **78**, 4253 (1997).
[25] R. Maezono, S. Ishihara, and N. Nagaosa, Phys. Rev. B **57**, R13993 (1998).
[26] F. Tsui, M. C. Smoak, T. K. Nath, and C. B. Eom, Appl. Phys. Lett. **76**, 2421 (2000).
[27] T. Kiyama, Y. Wakabayashi, H. Nakao, H. Ohsumi, Y. Murakami, M. Izumi, M. Kawasaki, and Y. Tokura, J. Phys. Soc. Jpn. **72**, 785 (2003).
[28] O. Chmaissem, B. Dabrowski, S. Kolesnik, J. Mais, J. D. Jorgensen, and S. Short, Phys. Rev. B **67**, 094431 (2003).
[29] The nuclear scattering length is 7.02×10^{-13} cm for Sr and 8.24×10^{-13} for La. This gives rise to a contrast between SMO and LMO unit cells of approximately 1.22×10^{-13} cm. The magnetic scattering length of a spin=3/2 moment is estimated to be 8×10^{-13} cm. For an *A*-type antiferromagnet, this gives rise to a magnetic contrast of 16×10^{-13} cm between layers. Since the observed intensity in scattering scales as the square of the contrast, the magnetic and nuclear peaks have a ratio of approximately $(16/1.2)^2$, which is more than 2 orders of magnitude.
[30] R. A. Cowley, Philos. Trans. R. Soc. London, Ser. A **354**, 2799 (1996).
[31] T. S. Santos, S. J. May, B. Kirby, B. B. Maranville, S. G. E. te Velthuis, J. Zarestky, and A. Bhattacharya (to be published).
[32] H. Kuwahara, T. Okuda, Y. Tomioka, A. Asamitsu, and Y. Tokura, Phys. Rev. Lett. **82**, 4316 (1999).